ADVANCES IN ATMOSPHERIC SCIENCES, VOL. 29, NO. 1, 2012, 91–100

# The Impact of Indian Ocean Variability on High Temperature Extremes across the Southern Yangtze River Valley in Late Summer

HU Kaiming[1,2] (胡开明), HUANG Gang*[3] (黄 刚),
QU Xia[1] (屈 侠), and HUANG Ronghui[1,2] (黄荣辉)

[1] *Center for Monsoon System Research, Institute of Atmospheric Physics, Chinese Academy of Sciences, Beijing* 100029

[2] *State Key Laboratory of Numerical Modeling for Atmospheric Sciences and Geophysical Fluid Dynamics, Institute of Atmospheric Physics, Chinese Academy of Sciences, Beijing* 100029

[3] *Key Laboratory of Regional Climate-Environment for East Asia, Institute of Atmospheric Physics, Chinese Academy of Sciences, Beijing* 100029

(Received 19 November 2010; revised 6 May 2011)

**ABSTRACT**

In this study, the teleconnection between Indian Ocean sea surface temperature anomalies (SSTAs) and the frequency of high temperature extremes (HTEs) across the southern Yangtze River valley (YRV) was investigated. The results indicate that the frequency of HTEs across the southern YRV in August is remotely influenced by the Indian Ocean basin mode (IOBM) SSTAs. Corresponding to June–July–August (JJA) IOBM warming condition, the number of HTEs was above normal, and corresponding to IOBM cooling conditions, the number of HTEs was below normal across the southern YRV in August. The results of this study indicate that the tropical IOBM warming triggered low-level anomalous anticyclonic circulation in the subtropical northwestern Pacific Ocean and southern China by emanating a warm Kelvin wave in August. In the southern YRV, the reduced rainfall and downward vertical motion associated with the anomalous low-level anticyclonic circulation led to the increase of HTE frequency in August.

**Key words**: high temperature extremes, tropical Indian Ocean, teleconnection

**Citation**: Hu, K. M., G. Huang, X. Qu, and R. H. Huang, 2012: The impact of Indian Ocean variability on high temperature extremes across the southern Yangtze River valley in late summer. *Adv. Atmos. Sci.*, **29**(1), 91–100, doi: 10.1007/s00376-011-0209-2.

## 1. Introduction

Extremely high temperatures can cause massive deaths, large-scale catastrophic crop failures, and shortages of water resources and power supplies (Haines et al., 2006; McMichael et al., 2006). These harmful effects are most obvious for densely populated regions, especially in the eastern part of China. For instance, daily mortality was significantly above normal in Shanghai during the summer heat waves in 1998 and 2003 (Tan et al., 2007). Thus, understanding the underlying causes and improving the forecast of such extreme events are important society and the economy.

A number of studies have been performed on the climatology and long-term trends in extreme temperature events in China. Using the Chinese observation station data set of the period 1951–1999, Zhai et al. (1999) and Su et al. (2006) detected a slightly decreasing trend in the number of hot days ($T_{\max} > 35°C$) in the Yangtze River valley (YRV). Whereas, there was an upward trend in the frequency and intensity of the HTE events in the northern part of China (north of

*Corresponding author: HUANG Gang, hg@mail.iap.ac.cn

40°N). Recently, by analyzing the climatological aspect as well as variability of the number of hot days in China during the period 1959–2008, Wei and Chen (2009) suggested that the standard deviation and average of the number of hot days were largest across the lower reaches of Yangtze River, with a maximum of 25 days in climatology and 15 days within standard deviation. The observational evidence gathered thus far have indicated that the frequency of high temperature extremes (HTEs) over eastern China shows significant variability on both the decadal and interannual time scales. The large interannual variability of the frequency means that heat waves are more likely in some years. For example, serious heat waves occurred in Shanghai in 1998 and 2003 (Tan et al., 2007). However, the interannual variability of number of HTEs is still not well understood.

The year-to-year variations of summer climate in China are largely controlled by variability in the East Asian summer monsoon (Huang, 2004). One of the key factors contributing to this interannual variability are the sea surface temperature anomalies (SSTAs; Yang et al., 2007; Huang and Hu, 2008; Li et al., 2008; Xie et al., 2009) due to the Indian Ocean basin mode (IOBM; Klein et al., 1999; Saji et al., 1999). The mechanism for this influence was revealed by Xie et al. (2009) and can be demonstrated as follows. IOBM SST warming forces a Matsuno–Gill (Matsuno, 1966; Gill, 1980) response in the tropospheric temperature. The warm tropospheric Kelvin wave propagates into the western Pacific and induces Ekman divergence in the subtropical Northwest Pacific Ocean (NWP), which in turn leads to suppressed convection and an anticyclonic circulation near the surface. The NWP anticyclone, with weak convection, leads to the summer rainfall anomalies in East Asia. Recent forecast experiments using a coupled general circulation model (GCM) also confirmed this tropical Indian Ocean teleconnection to the NWP and East Asia summer climate (Chowdary et al., 2009). Hence, the hypothesis that the IOBM pattern SSTAs have some implications for HTEs in China, especially in eastern China, has been reiterated in the present study.

The primary focus of this study was to delineate the relationship between IOBM SSTAs and HTEs in China and to reveal their underlying physical mechanism. This paper is organized as follows. The data sets are described in section 2. The observational evidence of the close relationship between Indian Ocean SSTAs and the HTEs across the southern YRV are shown in section 3. The mechanism for the impact of the IOBM SSTAs on HTEs in China is analyzed in section 4. The main conclusions of this work are summarized and discussed in section 5.

## 2. Data

The China daily maximum surface-temperature data set used in this study is an updated homogenized daily maximum and minimum temperature data set, which includes 730 stations in China for the period 1960–2008. A detailed description was documented by Li and Yan (2009). Following previous definition of Wei and Chen (2009), we defined an HTE as a day when the maximum temperature was >35°C.

The global precipitation data set used in this study was the monthly mean Climate Prediction Center (CPC) Merged Analysis of Precipitation (CMAP; Xie and Arkin, 1997), which is available (resolution: 2.5°×2.5°) starting in January 1979.

The global outgoing long-wave radiation (OLR) data was acquired from the Interpolated OLR data set (Liebmann and Smith, 1996), provided by the National Oceanic and Atmospheric Administration (NOAA). This OLR data set has data available (resolution: 2.5°×2.5°) starting in January 1979.

The SST data used in this study was the HadISST1 (Rayner et al., 2003), provided by the Hadley Center. This SST data set (resolution 1°×1°) and has data available from 1870 forward.

This study used winds, vertical velocity, surface sensible heat flux, surface latent heat flux, and air temperature from the National Centers for Environmental Prediction-National Center for Atmospheric Research (NCEP-NCAR) reanalysis data set (Kalnay et al., 1996). The monthly mean temperature advection at low levels derived from the NCEP daily winds and temperature was also used in this analysis. These data are available (resolution: 2.5°×2.5°) from 1948 forward.

To be consistent with the global precipitation data set, our study mainly focused on the impact of the IOBM on summer temperature anomalies in China during the period 1979–2008. An IOBM index was constructed by averaging the June–July–August (JJA) SSTs over the domain within 20°S–20°N, 40°–100°E. Throughout this study, analyses were performed for interannual variations on time scales shorter than 8 years. A linear trend was subtracted from raw anomalies to remove long time-scale variations. For a 30-year time series, a correlation coefficient of 0.31 and 0.36 represented the 90% and 95% confidence levels based on the student $t-$test, respectively.

## 3. The relationship between the IOBM and HTEs in the southern YRV

Figures 1a–c show the correlation monthly HTEs from Chinese observation stations with the IOBM in-

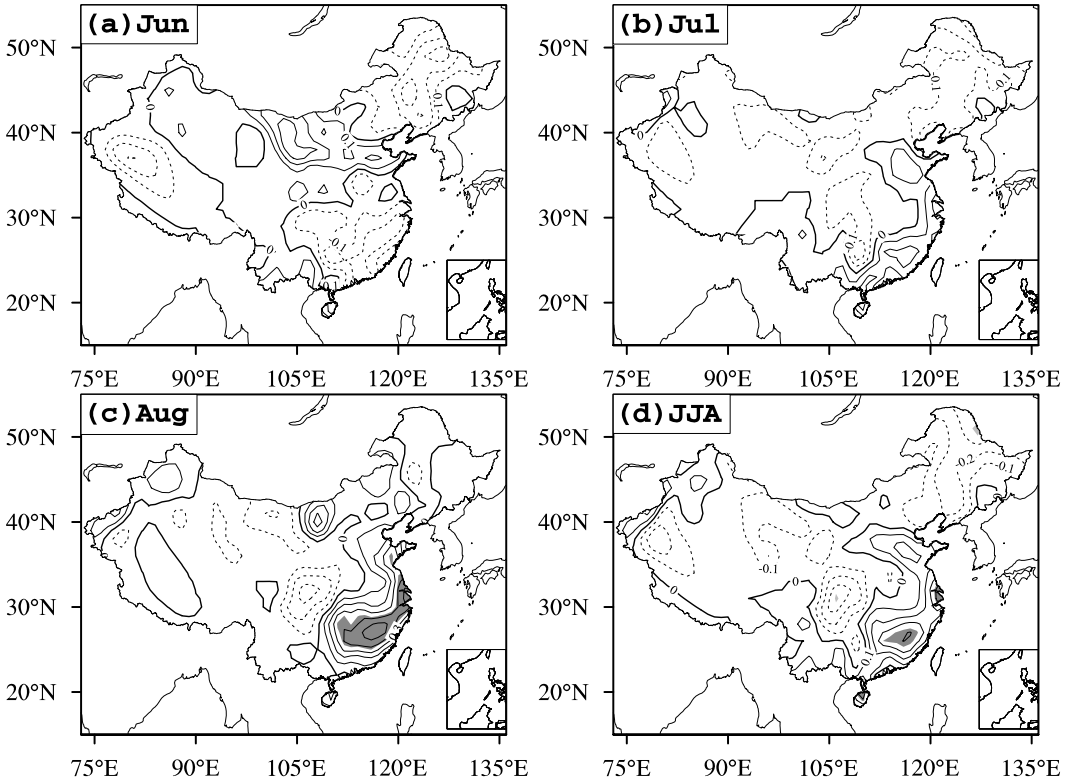


**Fig. 1.** Correlation of IOBM index with the number of HTEs in (a) June, (b) July, (c) August and (d) the JJA mean from the year of 1979 to 2008. The solid lines represent positive correlation and dash lines represent negative correlation, and the line interval at 0.1 in correlation. The shade areas denote 90% confidence level.

dex from June to August during the period 1979–2008. In June, a weak negative correlation was seen in southern China, the eastern part of central China, and Northeast China, and a weak positive correlation was seen in most of northern China. In July, the correlation was still weak, but the pattern was obviously different from June, having a positive correlation in the southern and eastern parts of China and a negative correlation in Northeast China and the western parts of central China. In August, by contrast, there were significant positive correlations in the southern YRV and the coastal region of eastern China, with the maximum coefficient >0.5. Among the correlation maps of these 3 months, it is important to note that correlation coefficients in the southern and eastern parts of China shifted from negative values in June to significantly positive values in August, suggesting that IOBM-induced HTE anomalies in the eastern and southern parts of China were not homogeneous during summer. Meanwhile, we calculated the correlation of mean HTEs in JJA with the IOBM index, which had a similar pattern but weaker correlation coefficients compared with those in August. These results demonstrate that it was necessary to divide the summer into the early summer (June), mid-summer (July), and late summer (August) when investigating the impacts of the IOBM on HTEs in China.

To further delineate the relationship between the IOBM and HTEs in the southern YRV, we calculated the number of HTEs [the average from all of the observation stations in the southern YRV (25° – −29°N, 112°–121°E)] in three scenarios: the climatology, IOBM warming years, and IOBM cooling years. One standard deviation signified an anomalous year. There were five IOBM warming years (1983, 1987, 1988, 1998, and 2003) and four cooling years (1984, 1985, 1989, and 2000) during the period 1979–2008. In Fig. 2, the HTEs in the southern YRV were confined to July and August. Moreover, the number of HTEs in each month was different in these three scenarios. In climatology, there were 3 HTEs in June, 15 HTEs in July, and 8.7 HTEs in August. In IOBM warming years, there were 2 HTEs in June, 17 HTEs in July, and 13.5 HTEs in August. For the cooling years, there were 3 HTEs in June, 12 HTEs in July, and 5.7 HTEs in August. Apparently, the difference of HTEs between Indian Ocean warming and cooling scenarios was most prominent in August. The results

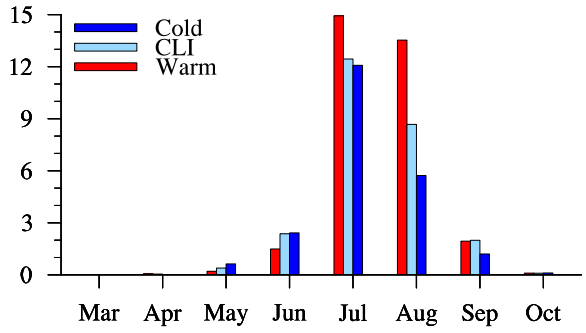


**Fig. 2.** Monthly number of HTEs in Climatology scenario (light blue), IOBM warming scenario (red) and IOBM cooling scenario (dark blue) in each month in the southern YRV, averaged in the region (25°–29°N, 112°–121°E).

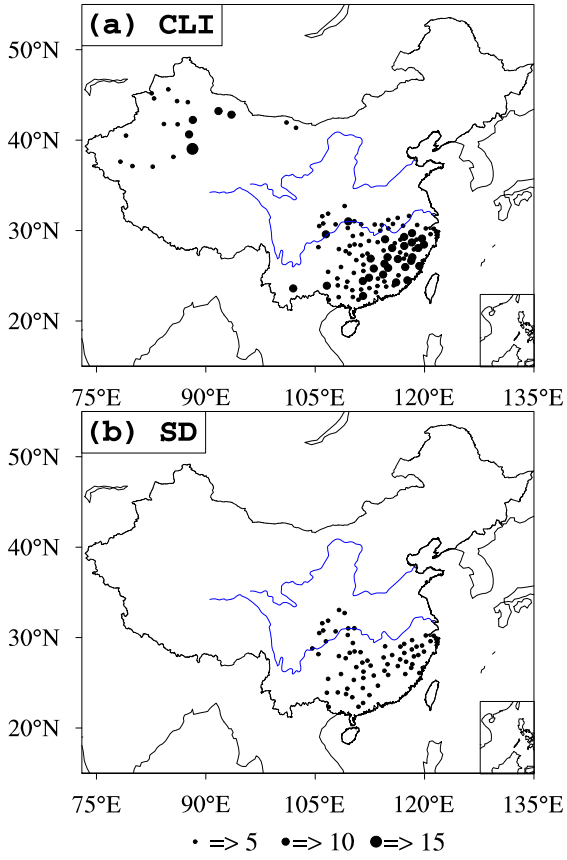


**Fig. 3.** (a) Climatology (average from 1979 to 2008) of the number of day with HTEs (with the maximum temperature greater than 35°C) across China in August. (b) The distribution of the standard deviation of HTEs in August over the period of 1979 to 2008. The diameter of a mark is proportional to the number of HTEs. The scales are shown in the bottom of panel.

were consistent with the correlation analysis in Fig. 1, indicating that the August HTEs in the southern YRV were closely related to IOBM SSTAs.

The spatial distribution of HTEs in China in August, the climatology and standard deviation of HTEs in August were examined (Figs. 3a and b, respectively). In addition to Northwest China, the largest HTEs were located in the southern and eastern parts of China, especially the southern YRV. Meanwhile, the largest standard deviations were also distributed in the southern YRV, with standard deviation ∼5 days. Thereby, the southern YRV was more vulnerable to HTEs during August. This relationship between IOBM SSTAs and HTEs in the southern YRV in August is an important one to study. In this study, two questions were proposed: First, what was the mechanism of the IOBM SSTAs impact on HTEs in the southern YRV? Second, why was this influence most significant in August? These two questions are discussed in the next section.

## 4. The possibility of a remote teleconnection from the tropical Indian Ocean to HTEs in the southern YRV

We studied the above two questions using three steps. First, we investigated the process of how IOBM-pattern SSTAs impact low-level circulation anomalies in East Asia. Secondly, we investigasted how IOBM-induced East Asia circulation anomalies impact HTEs in the southern YRV in August. Last, we studied the seasonal marches of IOBM-induced circulation anomalies in East Asia, and their impact on HTEs in the southern YRV from June to August.

### 4.1 *The impact of IOBM SSTAs on East Asia circulation anomalies in August*

The previous study of Xie et al. (2009) illustrated that IOBM SSTAs could affect the East Asian summer climate by propagating Kelvin waves. In this study, we investigated the impact of the IOBM on East Asian circulation anomalies in August. We calculated the correlations of 850-hPa wind velocity and tropospheric temperature (vertically averaged from 850 hPa to 200 hPa) in August with the IOBM index. As Fig. 4 shows, when Indian Ocean basin was warming, tropospheric temperature occurred in a Matsuno–Gill pattern, with the maximum correlation over the tropical Indian Ocean. A warm Kelvin-wave wedge penetrated into the western Pacific along the equator, with a pronounced anticyclonic circulation on its northern flank. With a low-level cyclonic circulation over central Japan, Korea, and Northeast China, a wave train propagated to a high latitude, signaling teleconnection like that of an East Asia–Pacific (EAP) teleconnection (Huang and Wu, 1989) and of a Pacific–Japan telecon-

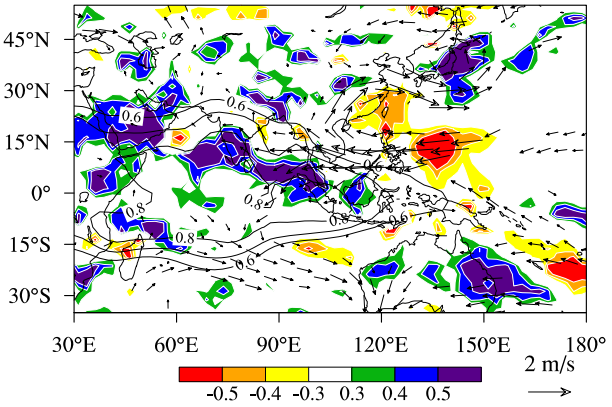


**Fig. 4.** Correlation with the IOBM index: precipitation (color) and tropospheric temperature (vertical average from 850 hPa to 200 hPa; contours) and regression of IOBM index on wind at 850 hPa (vectors) in August for the period of 1979 to 2008. Wind vectors denote the 90% confidence level.

nection (Nitta, 1987). Coupling with the circulation anomalies, the precipitation was below normal in southern China, and the surrounding seas where were controlled by anomalous anticyclones, and precipitation was above normal in the tropical Indian Ocean and central Japan. The results suggest that the IOBM-patterned SSTAs prominently affected the low-level circulation anomalies and precipitation anomalies over East Asia in August.

### 4.2 *The factors contributing to IOBM-induced HTEs in August*

HTEs are often caused by less precipitation, long-term sustaining circulation anomalies, radiation anomalies, and atmospheric downward motion. For example, the serious heat wave in Europe during 2003 was due to persistent anticyclonic conditions, lack of precipitation, radiation anomalies, downward motion and land–atmosphere feedback from May to August (Black et al., 2004; Fischer et al., 2007). Here, we investigated the IOBM-induced HTEs with regard to these factors.

Figures 5a and b show the correlation of IOBM index with precipitation, outgoing long-wave radiation (OLR) in August. The IOBM-precipitation correlation and IOBM-OLR correlation values were almost reversed signs. When we examined the southern YRV, this out-of-phase relationship was weak (shown in the rectangle in Fig. 5a). There were significant negative correlations between the IOBM index and precipitation, but there was a weak correlation between the IOBM index and the OLR. The negative correla-

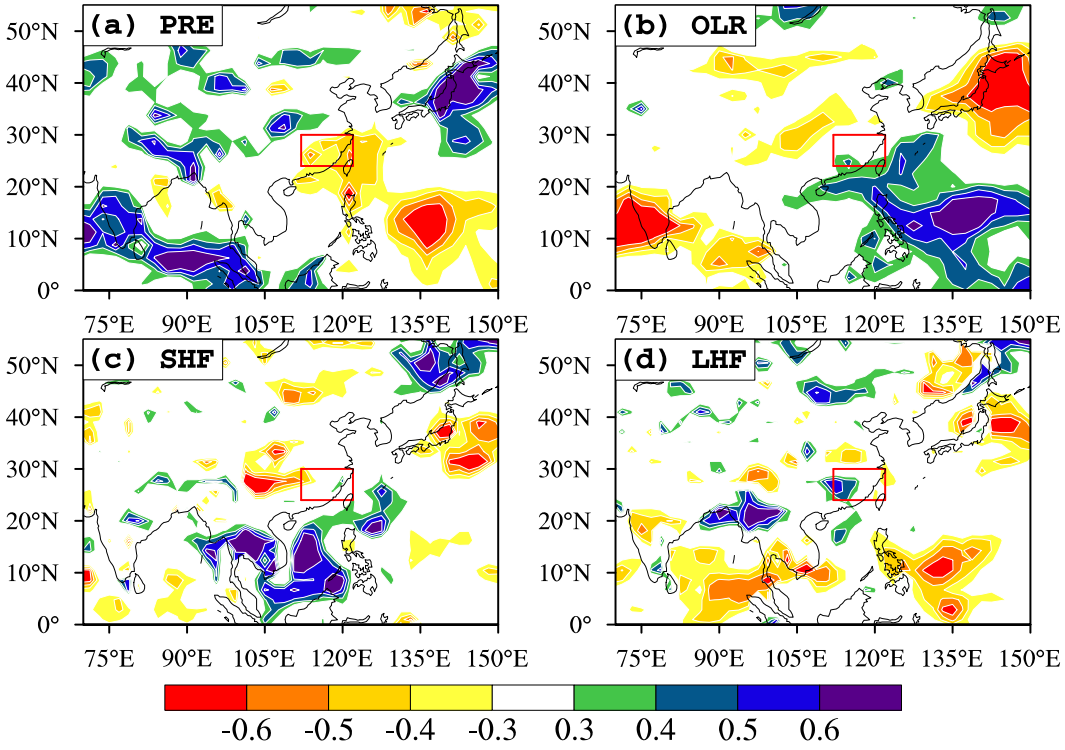


**Fig. 5.** Correlation of IOBM index with (a) precipitation, (b) outgoing longwave radiation, (c) surface sensible heat flux and (d) surface latent heat flux in August over the period 1979 to 2008. The rectangles in panel represent the region of the southern YRV.

tion between the IOBM index and precipitation was signified by the lack of rainfall in the southern YRV when the Indian Ocean was in its warming phase. And lack of rainfall may have contributed to the increase of HTEs in the southern YRV. Analogously, the lack of precipitation contributed to the heat wave in Europe in 2003 through changes in the land–atmosphere feedback (Fischer et al., 2007). Then, the lack of rainfall resulting from IOBM SSTAs was one of the factors contributing to HTEs in August. The weak correlation between IOBM and OLR suggests that the contributions of the IOBM-induced OLR to HTEs were weak (Fig. 5b). Figure 5c shows the correlation of IOBM with surface sensible heat flux (SHF) in August. The IOBM–SHF correlation pattern displays a significant triple structure from the South China Sea to higher-latitude regions, with positive correlations in the South China Sea and Northeast China and negative correlations in Japan and its nearby ocean. However, the correlation between IOBM and SHF were not significant in the southern YRV, suggesting a weak impact of IOBM-induced sensible heat flux anomalies on HTEs in the southern YRV. Figure 5c shows the correlation of the IOBM index with SHF in August. There were significantly positive correlations in the western part of the southern YRV. However, because the anomalies of SHF mainly represent the change in local evaporation, it is unclear whether or not the IOBM-induced SHF influenced local low-level air temperature.

The vertical temperature advection and horizontal temperature advection associated with IOBM SSTAs are shown in Figs. 6a and b. Like the data represented in Fig. 2, we chose five IOBM warming years and four IOBM cooling years, which were the same as those in section 3. We calculated daily horizontal and vertical temperature advection values in August, and we averaged them in the IOBM warming scenario and cooling scenarios, respectively. The differences of vertical and horizontal temperature advection between the IOBM warming scenario and the IOBM cooling sce-

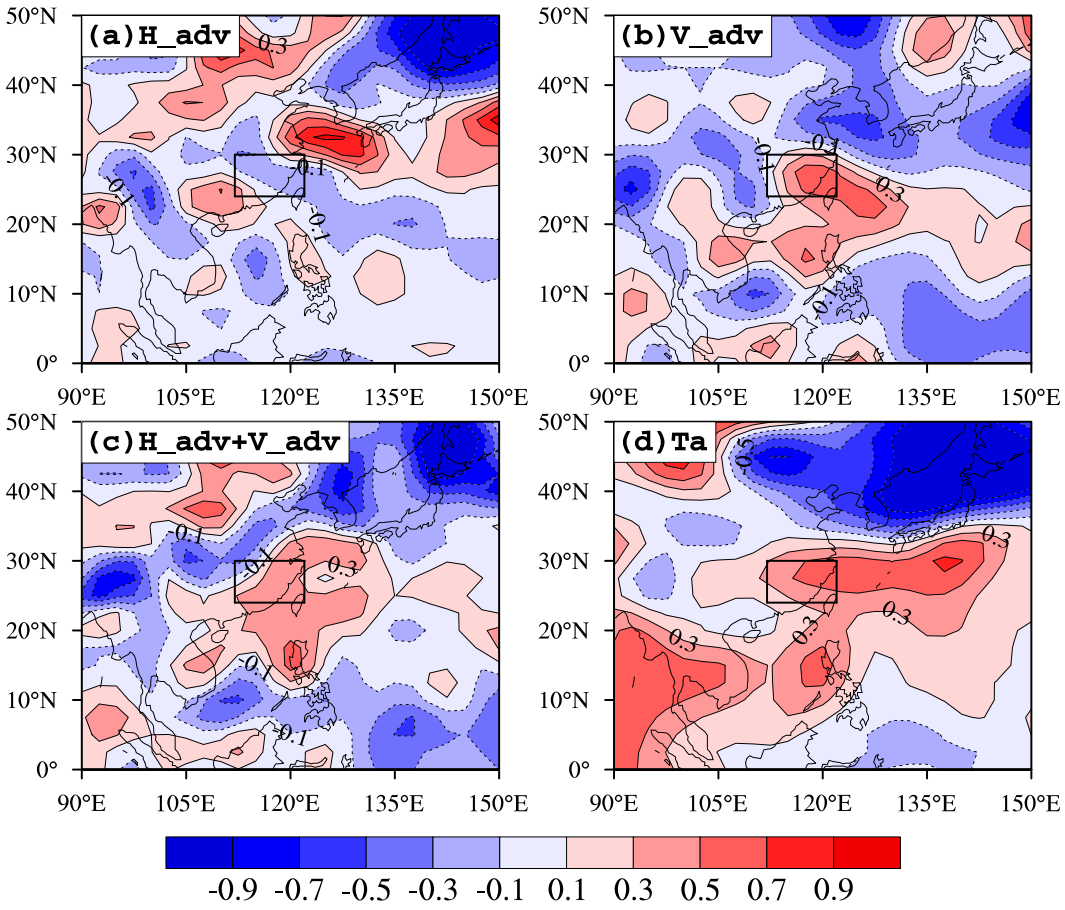


**Fig. 6.** The distribution of the difference of monthly mean low levels (vertical average from 1000 hPa to 850 hPa, units: K $d^{-1}$) (a) horizontal temperature advection (units: K $d^{-1}$), (b) vertical temperature advection (units: K $d^{-1}$), (c) their sum and (d) air temperature (units: K) between IOBM warming scenario and cooling scenario.

nario signified the IOMB-induced temperature advection anomalies. Because the terrain is complex in the southern YRV, we calculated vertical averages from 1000 hPa to 850 hPa to represent the low-level anomalies.

Figure 6a shows the IOBM-induced horizontal temperature advection anomalies at low levels. In the East Asia, the IOBM-induced horizontal temperature advection anomalies were characterized as wave structures extending northeastward from the Indochina peninsula to northern Japan. Negative temperature advection values occurred in the Indochina peninsula; positive values occurred in southwest China; negative values occurred in the southern YRV and positive values occurred in the belt from 30°N to 37°N; and negative values in the eastern part of Northeast China and northern Japan. These wave-like structures were associated with the EAP/PJ teleconnection pattern, with similar low-level circulation anomalies over East Asia resulting from SSTAs similar to an IOBM pattern. Focusing on the southern YRV, we observed a negative horizontal temperature advection belt over these regions of $< -0.1$ K d$^{-1}$. These results suggest that IOBM-induced, low-level, horizontal, temperature advection anomalies were not conducive to the increase of HTEs in the southern YRV region during August.

The IOBM-induced low-level vertical temperature advection anomalies are illustrated in Fig. 6b; they were also characterized as wave structures extending northward from the tropical western Pacific to high latitudes. Apparently, the structure of IOBM-induced vertical temperature advection anomalies was, to some extent, out of phase with horizontal temperature advection anomalies, especially in the coastal region of East Asia. For instance, they were above normal in the northern part of the Indochina peninsula, below normal in southwestern China, above normal in the southern YRV region, and below normal in the Bohai Sea, Korea, and Japan. Notably, in the southern YRV, the IOBM-induced, low-level, vertical temperature advection anomalies had larger amplitudes than did horizontal temperature advection anomalies, but with reversed signs. The positive IOBM-induced vertical temperature advection anomalies contributed to the increase of HTEs in the southern YRV during August.

The sum of vertical and horizontal temperature advection anomalies are shown in Fig. 6c. In tropical and subtropical regions, the pattern of total temperature advection anomalies was similar to the pattern of vertical temperature advection anomalies. In mid-latitudes, by contrast, the structure of total temperature advection anomalies was similar to the pattern of horizontal temperature advection anomalies. The results illustrate that the IOBM-induced vertical temperature advection anomalies were more prominent than were the horizontal temperature advection anomalies in tropical and subtropical regions, and their contrasting values were reversed in mid-latitude, possibility because the horizontal temperature gradient are larger in mid-latitude regions than subtropical. Notably, for the the southern YRV, the IOBM-induced total temperature advection anomalies were $>0.3$ K d$^{-1}$ over most of the region. The results suggest that IOBM-induced low-level horizontal and vertical temperature advection anomalies offset each other in the southern YRV, but that the vertical temperature advection anomalies were more prominent.

Moreover, we calculated the IOBM-induced low-level temperature anomalies during August (Fig. 6d). Apparently, the pattern of low-level temperature anomalies was consistent with total low-level temperature advection anomalies, with cooling anomalies in the tropical western Pacific and mid-latitudes of East Asia, and warming anomalies over the South China Sea and the southern YRV, indicating that IOBM-induced low-level temperature anomalies mainly resulted from the temperature advection anomalies.

Previous studies have revealed that the increase of climatologic temperature is closely related to enhanced HTEs. Thus, it was reasonable to study the impact of IOBM SSTAs on HTEs by examining IOBM-induced temperature anomalies. When the IOBM was warming, the low-level temperature was above normal in August over the southern YRV region, which was consistent with the increase of HTEs in this region. The low-level warming anomalies in the southern YRV were mainly due to vertical temperature advection anomalies. Meanwhile, the IOBM-induced precipitation and OLR were investigated, and our results show that the precipitation over the southern YRV was below normal when the IOBM was warming. Following these previous studies, the lack of rainfall may have contributed to HTEs by modulating land–air interactions. Furthermore, the precipitation anomalies and low-level temperature advection anomalies were associated with the circulation anomalies resulting from IOBM SSTAs.

Based on this investigation, we propose that the possible mechanism for the impact of IOBM-pattern SSTAs on China's surface temperature as follows. The IOBM SSTAs emanated a warm Kelvin wave into the Pacific in August. The Kelvin wave triggered suppressed convection and anomalous anticyclone circulation over the Northwest Pacific and southern China. In the southern YRV, anomalous anticyclone circulation contributed to above-normal low-level temperatures and the lack of rainfall through temperature advection and downward motion. And the warmer-than-

normal, low-level temperature and the lack of rainfall led to an increase in HTEs.

### 4.3 *The reason that IOBM-induced HTEs were most prominent in August*

The preceding section proposed a possible mechanism for the impact of IOBM pattern SSTAs on HTE anomalies in the southern YRV. But the reason that the impact of IOBM on HTE anomalies was most prominent in August is clarified in this section.

To delineate the detailed evolution of IOBM-induced NWP anticyclone and precipitation anomalies, longitudinal averages of precipitation and 850-hPa wind fields were computed at 5-d intervals. At a given latitude between the equator and 45°N, these averages were taken over a band with 20° longitudinal width (110°–130°E). The regression of 10 consecutive days and longitudinal average 850-hPa wind on the IOBM index and corresponding IOBM–precipitation correlation were plotted as a function of time and latitude (Fig. 7).

From 5 May to 30 September, there were three active periods of IOBM-induced anticyclone: 5–25 May, 10 June–5 July, and 25 June–1 September. In addition to this active–inactive–active character, the IOBM-induced anticyclone also featured a prominent northward march: the northern flank of this anomalous anticyclone leaped from ∼25°N to ∼30°N during early June, and it leaped from about 30°N to 35°N during late July. Corresponding to northward marching of the anomalous anticyclones, the IOBM-induced precipitation anomalies also extended northward from May to August. Generally speaking, above-normal precipitation was located in the northern flank of the anomalous anticyclone for moisture conveyance, and below-normal rainfall was suited in the ridge of the anticyclone for subsidence motion. Previous studies (Xie et al., 2009) revealed that IOBM SST warming was able to excite JJA mean anticyclone anomalies. In this study, these IOBM-induced anticyclones demonstrated prominent intraseasonal variation from early summer to late summer. Moreover, the time–latitude evolution of IOBM-induced circulation and precipitation anomalies was not continuous but had northward leaping and an active–inactive phase. Notably, the active–inactive phase change did not accurately correspond to calendar months. However, the second and third active phases of the IOBM-induced anticyclone and precipitation anomalies mainly occurred in June and August, and an inactive phase mainly occurred in July. Thus, it was reasonable to consider the impact of IOBM SSTAs on HTEs in June, July, and August, respectively.

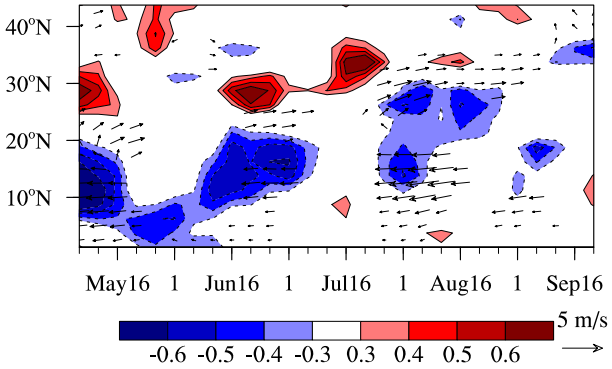


**Fig. 7.** Correlation of longitudinal averages of precipitation (color) over the 110°–130°E with IOBM index and regression of longitudinal averages of 850-hPa wind (vectors) over the 110°–130°E on IOBM index during the period 1979–2008 with latitude (ordinate) and pentad from 6 May to 21 September (abscissa). Patterns are based on a running average over 10 consecutive days.

When we examined the band from 24° to 30°N where the southern YRV was located, we noticed increased precipitation from 10 June to 5 July and reduced rainfall from 26 July to 1 September. The change of rainfall anomalies in this band was consistent with the northward march of the anomalous anticyclone. The results suggest that the southern YRV was controlled by the ridge of an IOBM-induced anticyclone from 25 July to 1 September, but they were controlled by the northern flank of an anticyclone from 10 June to 5 July. Based on the seasonal march of IOBM-induced precipitation and circulation anomalies, we investigated the impact of IOBM SSTAs on HTEs in the southern YRV in each month of summer. In June, the southern YRV was controlled by the northern flank of an anomalous anticyclone; the above-normal precipitation was not conducive to HTEs. In August, by contrast, the southern YRV was controlled by the ridge of an anomalous anticyclone, and the corresponding downward vertical motion and lack of rainfall were conducive to HTEs. Thus, the correlation between the IOBM index and the number of HTEs over the southern YRV was negative in June, but this value was significantly positive in August. In mid-July, the IOBM-induced anticyclone anomalies were inactive. Then, the impact of IOBM SSTAs on HTEs was weak.

## 5. Summary and discussion

We investigated the relationship between tropical IOBM SSTAs and the frequency of HTEs in China during summer. The results show that the relationship between the IOBM index and the number of HTEs across the southern YRV was most prominent

in August. Thereby, two questions were investigated in present study. First, how did the IOBM SSTAs impact the frequency of HTEs in the southern YRV? Second, why was the relationship between the IOBM index and the frequency of HTEs most prominent in August?

When the IOBM was warming, the tropospheric temperature anomalies displayed a Matsuno–Gill pattern corresponding to local SSTAs in August. The associated warm Kelvin ridge triggered low-level anticyclone anomalies over the NWP and southern China through Kelvin wave-induced Ekman divergence (WIED). The IOBM-induced anticyclone anomalies reduced precipitation and warm temperatures in the low-level troposphere in the southern YRV through downward vertical motion during August. Thus the frequency of HTEs in the southern YRV during August was above normal, when tropical IOBM was warming.

The IOBM-induced anomalous anticyclone had two active phases and marched northward from June to August. From June to early July, the southern YRV was located in the northern flank of IOBM-induced anomalous anticyclone, and rainfall increased. In mid-July, the IOBM-induced anticyclone anomalies were in an inactive phase. From late-July to August, the southern YRV was located on the ridge of IOBM-induced anomalous anticyclone, and rainfall amounts decreased. Thus, the impact of IOBM SSTAs on the frequency of HTEs in the southern YRV was most prominent in August.

This study focused on the impact of tropical Indian Ocean SSTAs on the frequency of HTEs in China through low-level circulation anomalies. The tropical Indian Ocean SSTAs may also have been able to influence the South Asia High (Yang et al., 2007; Huang et al., 2010), which may in turn have had implications for the HTEs through modulating upper-level circulation. The tropical Indian Ocean may also have exerted a significant influence on the temperatures of other parts of China, such as Northeast China (Hu et al., 2011). Moreover, the SSTAs in other regions also contributed to the variability of China circulation and temperature anomalies (Zhou and Chan, 2007; Wu et al., 2010). Prediction of the frequency of HTEs in China may also need to be comprehensively understood in terms of the contributions of different ocean and tropical intraseasonal oscillations (Zhou and Chan, 2005), which deserve further study.

***Acknowledgements.*** The authors are grateful to Prof. Shang-ping XIE and Prof. Renguang WU for helpful discussions and to two anonymous reviewers for their useful comments. This work was jointly supported by the National Basic Research Program of China 973 Projects (Grants Nos. 2012CB955604 and 2010CB950403), the Chinese Academy of Sciences (Grant No. XDA05090402), the National Special Scientific Research Project for Public Interest under Grant 20106021, and the National Natural Science Foundation of China (Grant Nos. 40890155, U0733002, 40730952, and 40810059005) .

## REFERENCES

Black, E., M. Blackburn, G. Harrison, B. Hoskins, and J. Methven, 2004: Factors contributing to the summer 2003 European heatwave. *Weather*, **59**, 217–223.

Chowdary, J. S., S. P. Xie, J. J. Luo, J. Hafner, S. Behera, Y. Masumoto, and T. Yamagata, 2009: Predictability of Northwest Pacific climate during summer and the role of the tropical Indian Ocean. *Climate Dyn.*, **1**, 169.

Fischer, E. M., S. I. Seneviratne, P. L. Vidale, D. Lüthi, and C. Schär, 2007: Soil Moisture–Atmosphere Interactions during the 2003 European Summer Heat Wave. *J. Climate*, **20**, 5081–5099.

Gill, A. E., 1980: Some simple solutions for heat-induced tropical cirulation. *Quart. J. Roy. Meteor. Soc.*, **106**, 447–462.

Haines, A., R. S. Kovats, D. Campbell-Lendrum, and C. Corvalan, 2006: Climate change and human health: Impacts, vulnerability, and mitigation. *The Lancet*, **367**, 2101–2109.

Hu, K. M., G. Huang, and R. H. Huang, 2011: The impact of tropical Indian Ocean variability on summer surface air temperature in China. *J Climate*, doi: 10.1175/2011JCLI4152.1. (in press)

Huang, G., 2004: An index measuring the interannual variation of the East Asian summer monsoon—The EAP index. *Adv. Atmos. Sci.*, **21**, 41–52.

Huang, G., and K. Hu, 2008: Impact of North Indian Ocean SSTA on Northwest Pacific lower layer anomalous anticyclone in summer. *Journal of Nanjing Institute of Meteorology*, **31**, 749–757. (in Chinese)

Huang, G., X. Qu, and K. Hu, 2010: The impact of the tropical Indian Ocean on South Asian High in boreal summer. *Adv. Atmos. Sci.*, **28**, 421–432.

Huang, R., and Y. Wu, 1989: The influence of ENSO on the summer climate change in China and its mechanism. *Adv. Atmos. Sci.*, **6**, 21–32.

Kalnay, E., and Coauthors, 1996: The NCEP/NCAR 40-year reanalysis project. *Bull. Amer. Meteor. Soc.*, **77**, 437–471.

Klein, S. A., B. J. Soden, and N. C. Lau, 1999: Remote sea surface temperature variations during ENSO: Evidence for a tropical atmospheric bridge. *J. Climate*, **12**, 917–932.

Li, S. L., J. Lu, G. Huang, and K. M. Hu, 2008: Tropical Indian Ocean basin warming and East Asian summer monsoon: A multiple AGCM study. *J. Climate*, **21**, 6080–6088.

Li, Z., and Z. W. Yan, 2009: Homogenized daily

mean/maximum/minimum temperature series for China from 1960–2008. *Atmos. Oceanic Sci. Lett*, **2**, 237–243.

Liebmann, B., and C. A. Smith, 1996: Description of a complete (interpolated) outgoing longwave radiation data set. *Bull. Amer. Meteor. Soc.*, **77**, 1275–1277.

Matsuno, T., 1966: Quasi-geostrophic motions in the equatorial area. *J. Meteor. Soc. Japan*, **44**, 25–43.

McMichael, A. J., R. E. Woodruff, and S. Hales, 2006: Climate change and human health: Present and future risks. *The Lancet*, **367**, 859–869.

Nitta, T., 1987: Convective activities in the tropical western Pacific and their impact on the Northern Hemisphere summer circulation. *J. Meteor. Soc. Japan*, **65**, 373–390.

Rayner, N. A., and Coauthors, 2003: Global analyses of sea surface temperature, sea ice, and night marine air temperature since the late nineteenth century. *J. Geophys. Res.*, **108**, 4407, doi: 10.1029/2002JD002670.

Saji, N. H., B. N. Goswami, P. N. Vinayachandran, and T. Yamagata, 1999: A dipole mode in the tropical Indian Ocean. *Nature*, **401**, 360–363.

Su, B. D., T. Jiang, and W. B. Jin, 2006: Recent trends in observed temperature and precipitation extremes in the Yangtze River basin, China. *Theor. Appl. Climatol.*, **83**(1–4), 139–151.

Tan, J., Y. Zheng, G. Song, L. Kalkstein, A. Kalkstein, and X. Tang, 2007: Heat wave impacts on mortality in Shanghai, 1998 and 2003. *International Journal of Biometeorology*, **51**, 193–200.

Wei, K., and W. Chen, 2009: Climatology and trends of high temperature extremes across China in summer. *Atmos. Oceanic Sci. Lett.*, **2**, 153–158.

Wu, R., S. Yang, S. Liu, L. Sun, Y. Lian, and Z. Gao, 2010: Changes in the relationship between Northeast China summer temperature and ENSO. *J. Geophys. Res.*, **115**, doi: 10.1029/2010D014422.

Xie, P., and P. A. Arkin, 1997: Global precipitation: A 17-year monthly analysis based on Gauge observations, satellite estimates, and numerical model outputs. *Bull. Amer. Meteor. Soc.*, **78**, 2539–2558.

Xie, S. P., K. M. Hu, J. Hafner, H. Tokinaga, Y. Du, G. Huang, and T. Sampe, 2009: Indian Ocean Capacitor Effect on Indo-Western Pacific Climate during the Summer following El Nino. *J. Climate*, **22**, 730–747.

Yang, J. L., Q. Y. Liu, S. P. Xie, Z. Y. Liu, and L. X. Wu, 2007: Impact of the Indian Ocean SST basin mode on the Asian summer monsoon. *Geophys. Res. Lett.*, **34**, L02708, doi: 10.1029/2006GL028571.

Zhai, P., A. Sun, F. Ren, X. Liu, B. Gao, and Q. Zhang, 1999: Changes of climate extremes in China. *Climatic Change*, **42**, 203–218.

Zhou, W., and J. C. L. Chan, 2005: Intraseasonal oscillations and the South China Sea summer monsoon onset. *Int. J. Climatol.*, **25**, 1585–1609.

Zhou, W., and J. C. L. Chan, 2007: ENSO and the South China Sea summer monsoon onset. *Int. J. Climatol.*, **27**, 157–167.